Journal of Statistical Physics, Vol. 55, Nos. 3/4, 1989

Behavior of a Quantum Particle in Contact with a Classical Heat Bath

P. Nielaba,[1] J. L. Lebowitz,[1,2] H. Spohn,[3] and J. L. Vallés[4]

Received July 13, 1988; revision received December 12, 1988

We investigate the behavior of a two-level quantum system in contact with a classical heat bath, e.g., a solute particle with internal degrees of freedom immersed in a solvent of massive particles. Using a combination of analytical and numerical methods, we obtain precise information about localization, time-displaced correlation functions, and the frequency-dependent susceptibility of such solute particles. We find that these quantities can have a strong dependence on the density of the solvent fluid, with the maximum changes from the behavior of the corresponding isolated quantum system occurring in many cases at very low densities. We compare the exact results with those obtained by path integral Monte Carlo. There is good agreement with the imaginary time correlations, but analytic continuation to real time proves elusive: even with the best numerical data on the former, we can only get very gross features of the latter.

KEY WORDS: Quantum particle; classical bath; two-level approximation; real-time correlation functions; frequency shift; path integral Monte Carlo; analytic continuation.

1. INTRODUCTION

Understanding how the properties of an isolated quantum system are modified by interactions with the environment is a problem of great theoretical as well as practical interest. Examples include the shifts and broadening of the energy levels of an atom or molecule immersed in a fluid or plasma and the motion of an electron in a liquid.[1-3] The simplest

[1] Department of Mathematics, Rutgers University, New Brunswick, New Jersey 08903.
[2] Department of Physics, Rutgers University, New Brunswick, New Jersey 08903.
[3] Theoretische Physik, Universität München, Munich, Federal Republic of Germany, and ITP, Santa Barbara, California 93106.
[4] Courant Institute of Mathematical Sciences, New York, New York 10012.

0022-4715/89/0500-0745$06.00/0

model of such effects occurs when the features of interest in the isolated system can be represented, at least approximately, by a two-level quantum system, e.g., the inversion transition in an NH_3 (or similar) molecule[4] and the bistable Josephson tunnel junction.[5,6] Questions of interest for such systems are the effective tunneling rates, including possible localization in one of the two minima, energy absorption spectra, etc.

In this paper we study such phenomena for the case of a bistable quantum system interacting with a classical environment via short-range potentials. More specifically, we will think of our system as the limit of a model quantum particle in a double-well external potential immersed in a classical fluid. We assume for simplicity that the quantum particle moves only in one dimension, say along the x axis, while the fluid particles are in three dimensions. The appropriate model Hamiltonian is then

$$\hat{H} = \frac{p^2}{2m_0} + V(\mathbf{q}) + \sum_j \frac{1}{2M} p_j^2 + \frac{1}{2} \sum_{i \neq j} \tilde{U}(\mathbf{q}_i - \mathbf{q}_j) + \sum_j U(\mathbf{q} - \mathbf{q}_j) \tag{1.1}$$

Here $\mathbf{q} = (q, 0, 0)$ is the position and p the momentum of the quantum particle with mass m_0, and V is the external double-well potential. $\{\mathbf{q}_j, \mathbf{p}_j\}$ are the positions (in $\mathbb{R}^3$) and momenta of the fluid molecules with mass M. These interact with each other via the potential $\tilde{U}$ and with the quantum system via the potential U. The whole system is in thermal equilibrium at temperature T with fluid density ρ.

We assume now that the thermal wavelength of the fluid particles is small and that the typical time scale of the quantum system is much faster than the time scale set by the motion of the fluid molecules. The fluid may then be treated classically. Both of these requirements will be satisfied when the mass of the fluid particles M becomes very large (see ref. 7 and references there for related models with both quantum and classical degrees of freedom). Thus, we model the bistable quantum system as immersed in a *quasistatic, fluctuating* medium. With these simplifications the relevant quantum part of the Hamiltonian becomes, in units in which $\hbar = 1$,

$$H = -\frac{1}{2m_0} \Delta + V(\mathbf{q}) + \sum_j U(\mathbf{q} - \mathbf{q}_j) \tag{1.2}$$

where the $\{\mathbf{q}_j\}$ specify the fixed, time-independent, configuration of the classical particles.

H is a one-particle Hamiltonian with a *random* potential: the surrounding fluid modifies the bistable potential in an irregular fashion. The assumption that the original system (1.1) is in thermal equilibrium implies that averages for this quantum system have to be taken according to the

annealed prescription. Thus, if A and B are observables, then their time-displaced equilibrium correlation is defined by

$$\langle B(t)A\rangle_a = \frac{\langle \mathrm{Tr}[e^{-\beta H}e^{itH}Be^{-itH}A]\rangle}{\langle \mathrm{Tr}[e^{-\beta H}]\rangle} \tag{1.3}$$

where β is the reciprocal temperature and $\langle\cdot\rangle$ denotes the (classical) thermal average over the coordinates of the fluid particles. This is defined by

$$\langle f(\cdot)\rangle = \frac{\int_A \cdots \int_A d\mathbf{q}_1 \cdots d\mathbf{q}_N f(\cdot) \exp[-\frac{1}{2}\beta \sum_{i\neq j=1}^N \tilde{U}(\mathbf{q}_i - \mathbf{q}_j)]}{\int_A \cdots \int_A d\mathbf{q}_1 \cdots d\mathbf{q}_N \exp[-\frac{1}{2}\beta \sum_{i\neq j=1}^N \tilde{U}(\mathbf{q}_i - \mathbf{q}_j)]} \tag{1.4}$$

when there are N fluid particles in a region A. If the system is open or large compared to the range of V and U, then we can take $\langle\cdot\rangle$ to be a grand-canonical average at the appropriate fugacity z. Note that if $B=1$, then (1.3) defines the static equilibrium average of A. We can also rewrite (1.3) for any observable A in the form

$$\langle A\rangle_a = \int_A \cdots \int_A d\mathbf{q}_1 \cdots d\mathbf{q}_N \langle A\rangle_Q \mu(\mathbf{q}_1,\ldots,\mathbf{q}_N) \equiv \langle\langle A\rangle_Q\rangle_\mu \tag{1.5}$$

where

$$\langle A\rangle_Q = \frac{\mathrm{Tr}[e^{-\beta H}A]}{\mathrm{Tr}[e^{-\beta H}]} \tag{1.6}$$

is the normalized quantum expectation value for a fixed configuration $\{\mathbf{q}_i\}$ and the equilibrium average is modified to the new probability distribution μ given by

$$\mu(\mathbf{q}_1,\ldots,\mathbf{q}_N) = \frac{\exp[-\frac{1}{2}\beta \sum_{i\neq j=1}^N \tilde{U}(\mathbf{q}_i - \mathbf{q}_j)]\,\mathrm{Tr}[\exp(-\beta H)]}{\int_A \cdots \int_A d\mathbf{q}_1 \cdots d\mathbf{q}_N \exp[-\frac{1}{2}\beta \sum_{i\neq j=1}^N \tilde{U}(\mathbf{q}_i - \mathbf{q}_j)]\,\mathrm{Tr}[\exp(-\beta H)]} \tag{1.7}$$

We shall also consider averages in which the factors $\mathrm{Tr}(e^{-\beta H})$ are omitted from the above formula, so that $\mu \propto \exp[-\frac{1}{2}\beta \sum \tilde{U}(\mathbf{q}_i - \mathbf{q}_j)]$, as if the classical part of the system were not affected by the quantum part. Averages of this type will be called "quenched" averages; the ones with μ given by (1.7) will be called "annealed" averages. We may also take for μ any other *a priori* distribution. We shall use the notation $\langle\langle A\rangle_Q\rangle_\mu$ for all such cases.

It is clear from (1.5) that if the quantum average $\langle A \rangle_Q$ can be done for arbitrary configurations $\{\mathbf{q}_i\}$, then the remaining average is purely classical and can be done by standard Monte Carlo techniques. When this is not possible we can still evaluate annealed expectation values of static or imaginary time correlations, replacing t by $-i\tau$ in (1.3), by a path integral Monte Carlo (PIMC); for quenched averages this is more difficult. Once the PIMC calculation has been done, it is then possible *in principle* to analytically continue these correlations to real time.[7] It was one of the motives of this work to see how well this continuation works in practice.

The organization of the remainder of the paper is as follows. In the next section we approximate H in (1.2) by that of a two-level quantum system, corresponding to the two lowest levels in the bistable potential V. In Section 3 we present some exact results for the behavior of this two-level system in the thermal environment of a simplified model fluid. In Section 4 we present results on the imaginary-time correlations for this system obtained via PIMC and discuss the difficulties encountered in trying to analytically continue them to real times. In the last section we discuss the general imaginary-time Feynman path formalism for systems described by (1.2).

2. THE TWO-LEVEL APPROXIMATION

As indicated in the Introduction, we are interested in potentials V which have two symmetric pronounced minima at q_+ and q_-. Therefore at sufficiently low temperatures we can approximate our system (1.2) by a two-level system, corresponding to the symmetric and antisymmetric wave functions.[4,5] This system can now be represented by the usual spin-half Heisenberg Hamiltonian

$$H_s = -\tfrac{1}{2}\omega_0 \sigma^x - \tfrac{1}{2} h(\{\mathbf{q}_j\})\sigma^z + \tfrac{1}{2} u_0(\{\mathbf{q}_j\}) \tag{2.1}$$

where ω_0 is the energy difference between the two levels for the isolated system, and $\sigma^z = \pm 1$ corresponds to localization at $q_\pm$. The potentials

$$h(\{\mathbf{q}_j\}) = \sum_{j=1}^{N} [U(q_- - \mathbf{q}_j) - U(q_+ - \mathbf{q}_j)] \tag{2.2a}$$

and

$$u_0(\{\mathbf{q}_j\}) = \sum_{j=1}^{N} [U(q_- - \mathbf{q}_j) + U(q_+ - \mathbf{q}_j)] \tag{2.2b}$$

are produced by the fluid particles. Note that we have neglected here the effect of the bath on the tunneling frequency ω_0. As a consequence, the

interactions always increase the energy difference between the ground state and excited states

$$\omega_0 \to [\omega_0^2 + h^2]^{1/2} \equiv \Omega = (\tfrac{1}{2}u_0 + \tfrac{1}{2}\Omega) - (\tfrac{1}{2}u_0 - \tfrac{1}{2}\Omega) \tag{2.3}$$

corresponding to a "blue shift" of the absorption frequency. An analysis using directly the solution of the continuum Schrödinger equation for the Hamiltonian (1.2) which correctly treats this effect will be presented elsewhere.

Using (2.1), it is easy to compute the quantum averages $\langle A \rangle_Q$ defined in (1.6) for all quantities of interest. We find

$$\langle \sigma^x \rangle_Q = (\omega_0/\Omega) \tanh(\beta\Omega/2) \tag{2.4}$$

$$\langle \sigma^y \rangle_Q = 0 \tag{2.5}$$

$$\langle \sigma^z \rangle_Q = (h/\Omega) \tanh(\beta\Omega/2) \tag{2.6}$$

Let $C_Q^\alpha(t)$ denote the quantum mechanical expectation value for the σ^α-time correlation functions,

$$C_Q^\alpha(t) = \langle \sigma^\alpha(t)\sigma^\alpha \rangle_Q = \frac{\mathrm{Tr}[e^{-\beta H_s} e^{itH_s}\sigma^\alpha e^{-itH_s}\sigma^\alpha]}{\mathrm{Tr}[e^{-\beta H_s}]} \tag{2.7}$$

where $\alpha = x, y, z$, with $-\infty < \mathrm{Re}(t) < \infty$, $0 \leqslant -\mathrm{Im}(t) < \beta$. Then, using the eigenfunctions $\psi_{1,2}$ and eigenvalues $\lambda_{1,2}$ of H_s and utilizing

$$\begin{aligned}
&\sum_{j=1}^{2} \langle \psi_j | e^{-\beta H_s} e^{itH_s}\sigma^\alpha e^{-itH_s}\sigma^\alpha \psi_j \rangle \\
&\quad = \sum_{j,k=1}^{2} \langle \psi_j | e^{-\beta H_s} e^{itH_s}\sigma^\alpha e^{-itH_s}\psi_k \rangle \langle \psi_k | \sigma^\alpha \psi_j \rangle \\
&\quad = \sum_{j,k=1}^{2} e^{-\beta\lambda_j} e^{i(\lambda_j - \lambda_k)t} \langle \psi_j | \sigma^\alpha \psi_k \rangle \langle \psi_k | \sigma^\alpha \psi_j \rangle
\end{aligned}$$

we obtain for $C_Q^\alpha(t)$

$$C_Q^x(t) = \frac{\omega_0^2 + h^2 C_Q^y(t)}{\Omega^2} \tag{2.8}$$

$$C_Q^y(t) = \frac{\cosh[(\Omega/2)(\beta - 2it)]}{\cosh(\beta\Omega/2)} \tag{2.9}$$

$$C_Q^z(t) = \frac{h^2 + \omega_0^2 C_Q^y(t)}{\Omega^2} \tag{2.10}$$

Equations (2.8)–(2.10) also yield the frequency-dependent susceptibilities as defined by linear response theory.[8] Thus, the yy susceptibility is given by

$$\tilde{\chi}_Q^{yy}(\omega) = \int_0^\beta d\tau\, C_Q^y(-i\tau) - i\omega \int_0^\infty dt\, e^{-i\omega t} \int_0^\beta d\tau\, C_Q^y(t - i\tau) \tag{2.11}$$

The imaginary part of $\tilde{\chi}_Q^{yy}(\omega)$ is given by

$$\chi_Q^{yy}(\omega) = -\mathrm{Im}[\tilde{\chi}_Q^{yy}(\omega)] = \pi[\delta(\omega - \Omega) - \delta(\omega + \Omega)] \tanh(\beta\Omega/2) \tag{2.12}$$

For $\omega = 0$ we obtain $\tilde{\chi}_Q^{yy}(0) = 2\tanh(\beta\Omega/2)/\Omega$.

We can interpret these susceptibilities as the line shapes which would be observed for an isolated system. To obtain the susceptibility for a dilute solution of such a two-level system in the fluid, we need to average them over some distribution of the fluid particles.

Replacing H by H_s in (1.7), we obtain the distribution μ (corresponding to annealed averages)

$$\mu(\mathbf{q}_1, \ldots, \mathbf{q}_N) = \frac{\exp(-\beta H_{\mathrm{eff}})}{\int_A \cdots \int_A d\mathbf{q}_1 \cdots d\mathbf{q}_N \exp(-\beta H_{\mathrm{eff}})} \tag{2.13a}$$

where

$$H_{\mathrm{eff}} = \sum_{i<j} \tilde{U}(\mathbf{q}_i - \mathbf{q}_j) + \tfrac{1}{2} u_0(\{\mathbf{q}_k\}) - \frac{1}{\beta} \ln\left(\cosh\frac{\beta\Omega}{2}\right) \tag{2.13b}$$

In order to proceed further, we have to specify U and $\tilde{U}$. For the Monte Carlo calculations we choose for U the screened polarization potential

$$U(q) = W \frac{e^{-\kappa|q|}}{(q^2 + \alpha^2)^2} \tag{2.14a}$$

with (for numerical convenience) $W = -5\omega_0$, $\alpha = \sqrt{2}$, and $\kappa = 3$, in units in which $q_\pm = \pm 1$. For the interaction between the fluid particles we choose a simple hard-core potential. The role of this potential is primarily to prevent excessive concentrations of fluid particles in the vicinity of the quantum particle (see Section 5). For this reason we actually simplified the model further by replacing, in most computations, the continuum fluid by a hard-core lattice gas on a simple cubic lattice with lattice spacing $b = 0.5$ and the particles occupying the centers of cubes with *a priori* probability p. For the analytical calculations, which were carried out using a lattice gas

model with lattice spacing $b=0.5$, we use, instead of the potential in (2.14a),

$$U(q)=\begin{cases} U_0 & \text{if } |q|\leqslant 0.5 \\ 0 & \text{if } |q|>0.5 \end{cases} \tag{2.14b}$$

with U_0 chosen so that (2.14a) and (2.14b) agree when $|q|=0.5$.

3. RESULTS OF ANALYTIC CALCULATIONS

Before describing the results of our computations on the effects of the environment, we note that for the isolated system the equilibrium density matrix is diagonal in the σ^x representation, so that $\langle\sigma^z\rangle_Q=0$ and $\langle\sigma^x\rangle_Q=\tanh(\frac{1}{2}\beta\omega_0)$. Similarly, with

$$C_\alpha(t)=\langle C_Q^\alpha(t)+C_Q^\alpha(-t)\rangle_\mu/2 \qquad (\alpha=x,\ y,\ x)$$

denoting the symmetrized time correlation functions, $C_x(t)=1$, while $C_z(-i\tau)$ has a minimum at $\tau=\beta/2$, where its value is given by $\cosh(\beta\omega_0/4)/\cosh(\beta\omega_0/2)$. The effect of the fluid is to "hybridize" these eigenstates, i.e., the new eigenstates will be a linear combination of the σ^x eigenstates, since the quantum system can lower its energy (for some configurations $\mathbf{q}$) by being in an eigenstate of σ^z. Thus, for $\beta\to\infty$, $\langle\sigma^z\rangle_Q=h/\Omega\sim\pm1$ for configurations in which $|h|\gg\omega_0$, i.e., ones in which there is a large difference in the potentials at $q_\pm$. This would correspond to approximate localization of the particle in one of the potential minima at $q_\pm$. To obtain quantitative results about the degree of localization, energy shifts, etc., as a function of density and temperature, we have to carry out the classical average with μ given by (2.13). This average can be done analytically when the fluid particles on different lattice sites do not interact and U is given by (2.14b). There are then eight sites around each of the minima at q_+ and q_-, and $\langle\cdot\rangle_\mu$ involves weighted sums over 2^{16} configurations; due to symmetry, Ω can take only nine different values. The results obtained this way are very similar qualitatively to those obtained without truncation by Monte Carlo evaluation of $\langle\cdot\rangle_\mu$.

This can be seen in Figs. 1–3, where we show graphs of the $C_\alpha(-i\tau)$ versus τ/β for $\alpha=x,\ y,\ z$ at various lattice densities.

In our calculation we set $\beta=16\omega_0^{-1}$. A striking feature of these graphs is that the strongest hybridization, as measured by the rise in value $C_z(-i\tau)$ at its minimum, when $\tau=\beta/2$ [remember that $C_z(-i\tau)=1$ when the system is dominated entirely by the interactions] occurs at very low densities: this value of C_z is plotted in Fig. 4. For the nearest neighbor case we find that the maximum occurs at a lattice gas density $\bar{p}(\beta)$ given by

$$\bar{p}(\beta)=\tfrac{1}{2}[1+\tanh(\beta u_{\min}/4)]\xrightarrow[\beta\to\infty]{}\tfrac{1}{2}[1+\operatorname{sign}(u_{\min})] \tag{3.1}$$

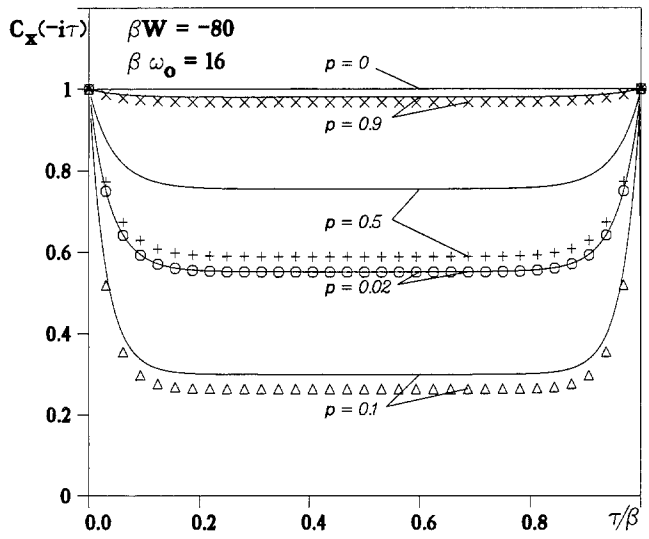

Fig. 1. Imaginary-time correlation functions $C_x(-i\tau)$. Comparison of the nearest neighbor summation (lines) with the Monte Carlo simulations. (○) $p \sim 0.02$, (△) $p \sim 0.1$, (+) $p = 0.5$, (×) $p \sim 0.9$.

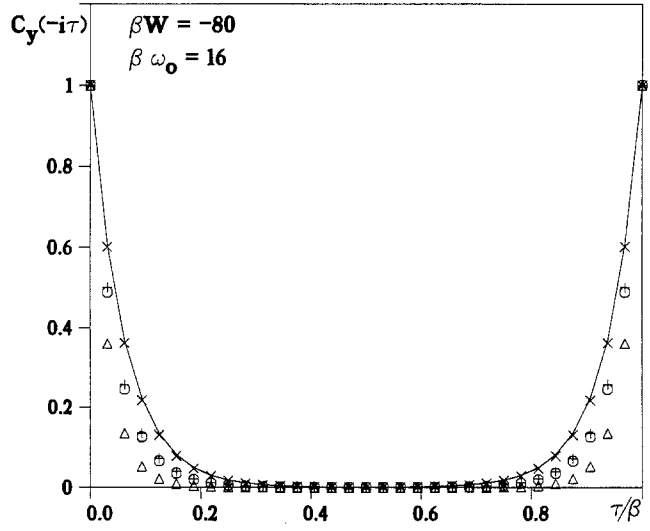

Fig. 2. Imaginary-time correlation functions $C_y(-i\tau)$. Monte Carlo simulations (symbols as in Fig. 1), solid line for $p = 0$.

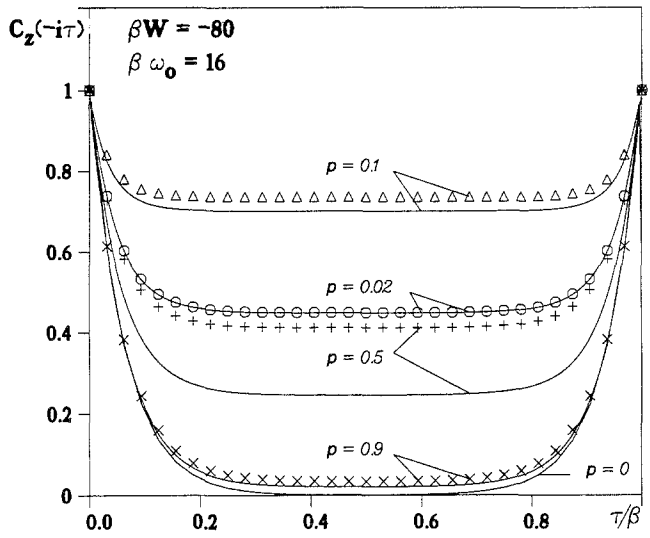

Fig. 3. Imaginary-time correlation functins $C_z(-i\tau)$. Comparison of the nearest neighbor summation (lines) with the Monte Carlo simulations (symbols as in Fig. 1).

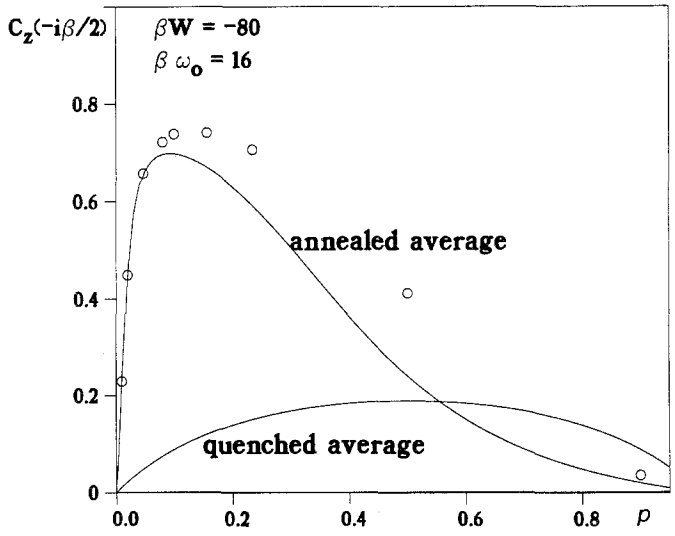

Fig. 4. Value of the σ^z imaginary-time correlation functions at $\beta/2$ as a function of the density. Comparison of the nearest neighbor summation (lines) with Monte Carlo simulations (○). We also put in there the same quantity for the nearest neighbor summation for a quenched distribution of fluid particles; see Eq. (1.7).

where $u_{\min}$ is the value of the potential u_0 when all the lattice sites near the quantum particle are occupied, see Fig. 5. We also see from Eq. (2.10) that

$$\lim_{\substack{\beta \to \infty \\ p = \bar{p}(\beta)}} C_z(-i\beta/2) = h^2_{\max}/\Omega^2_{\max} \sim 0.839 \tag{3.2}$$

where the maximum values of h and Ω are computed from (2.2a) and (2.3). The small value of $\bar{p}$ at large β is somewhat unexpected and is an effect of using the annealed average. For quenched averages, where μ would be just a product measure over different lattice sites, with occupation probability p, the maximum would be expected to occur at $p = 1/2$, where the fluctuations in the density are largest. A plot of $C_z(-i\beta/2)$ for the quenched case with $p = 1/2$ is also shown in Fig. 4. Note that in this case

$$\lim_{\substack{\beta \to \infty \\ p = 1/2}} C_z(-i\beta/2) = \langle h^2/\Omega^2 \rangle_\mu \neq 0 \tag{3.3}$$

$p = 1/2$, where the average is now with respect to the quenched measure. There are thus considerable differences in the behavior of the quantum system in an annealed and a quenched environment. Similar differences should exist also in more realistic situations and it would be interesting to find experimental examples of this phenomenon.

In Figs. 6–8 we show the real-time correlation functions. Since they are obtained by averaging over a finite number of values of Ω, these functions

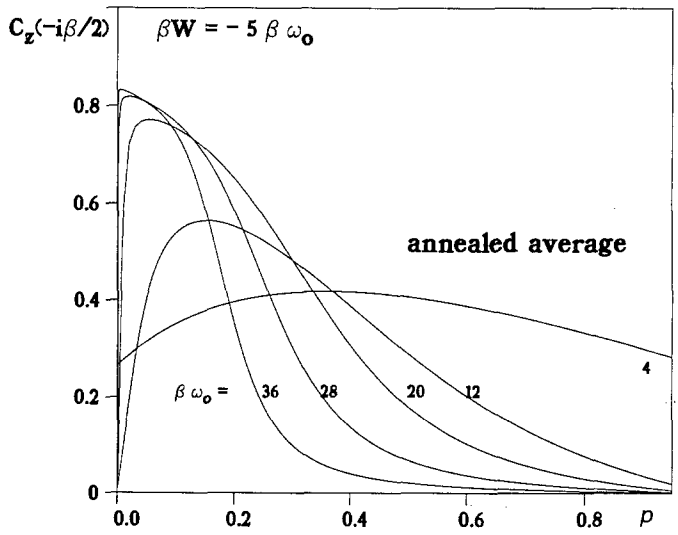

Fig. 5. Value of the σ^z imaginary-time correlation functions at $\beta/2$ for different values of β as a function of the density. Results of the nearest neighbor summation for various values of $\beta\omega_0 = 4$, 12, 20, 28, 36 from top to bottom at $p = 0.6$.

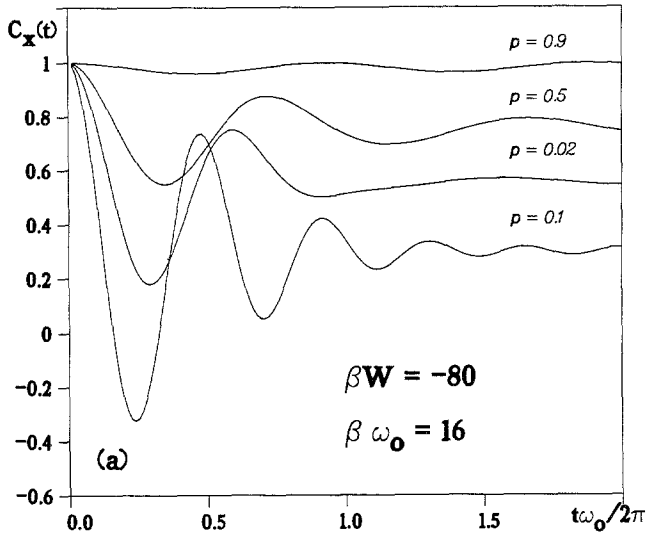

(a)

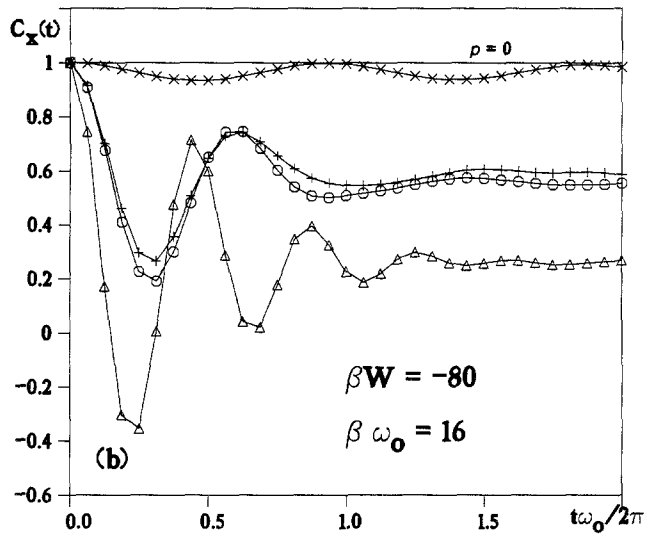

(b)

Fig. 6. The σ^x real-time correlation functions for various densities of the classical particles. (a) Nearest neighbor summation. (b) Monte Carlo simulation (symbols as in Fig. 1, connected by lines for visual guidance), solid line for $p = 0$.

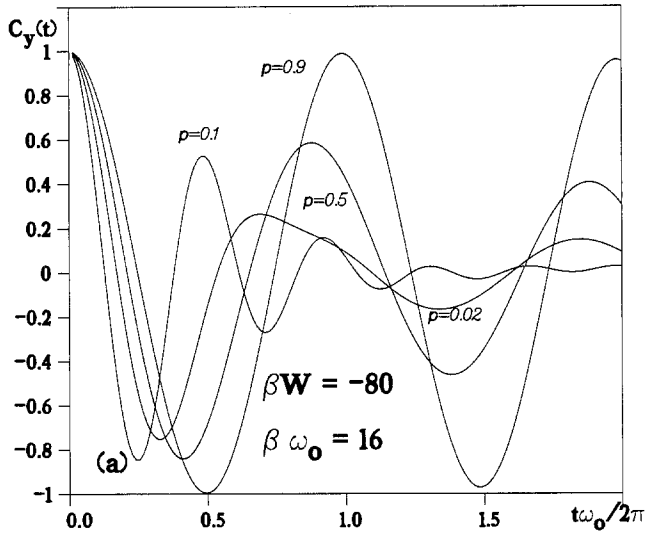

(a)

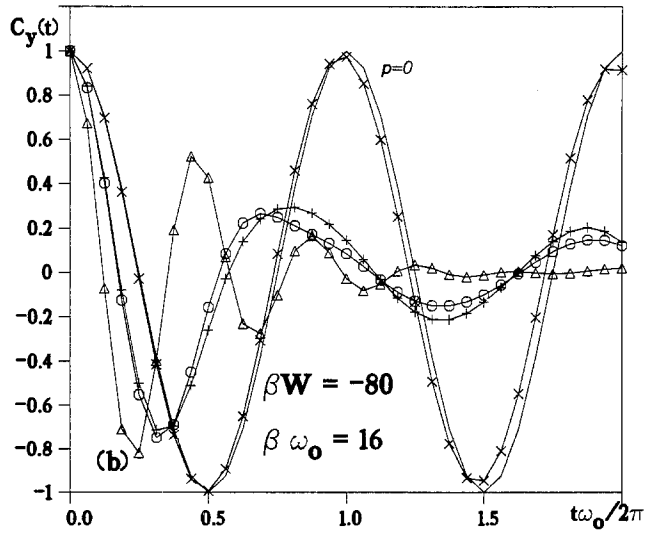

(b)

Fig. 7. The σ^y real-time correlation functions for various densities of the classical particles. (a) Nearest neighbor summation. (b) Monte Carlo simulation (symbols as in Fig. 1, connected by lines for visual guidance), solid line for $p = 0$.

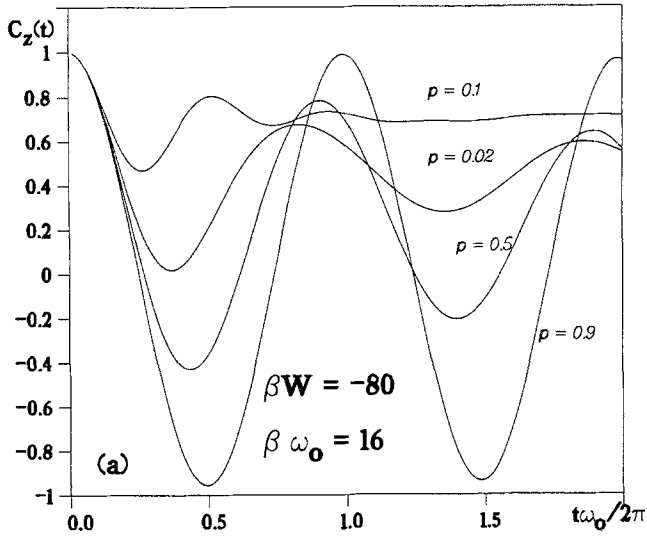

(a)

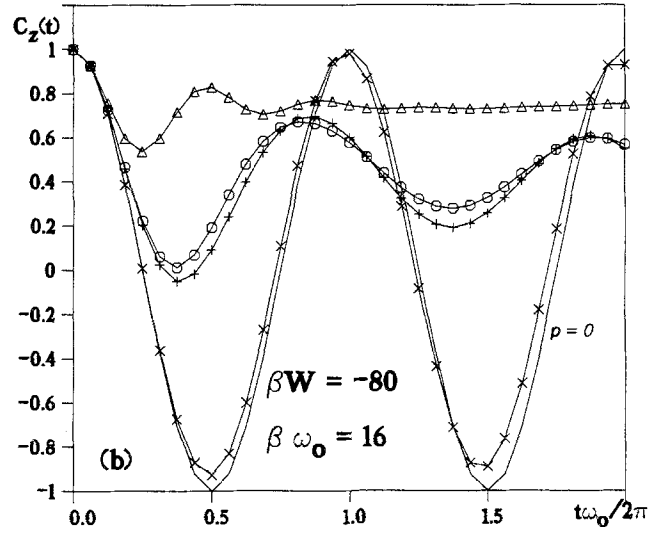

(b)

Fig. 8. The σ^z real-time correlation functions for various densities of the classical particles. (a) Nearest neighbor summation. (b) Monte Carlo simulation (symbols as in Fig. 1, connected by lines for visual guidance), solid line for $p = 0$.

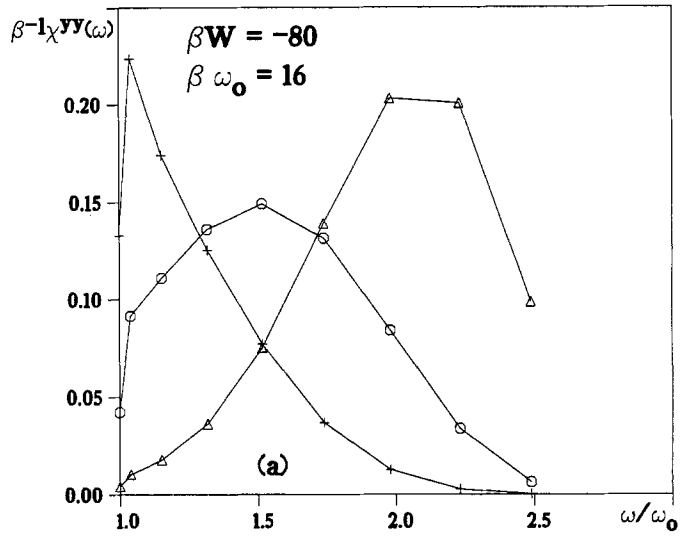

(a)

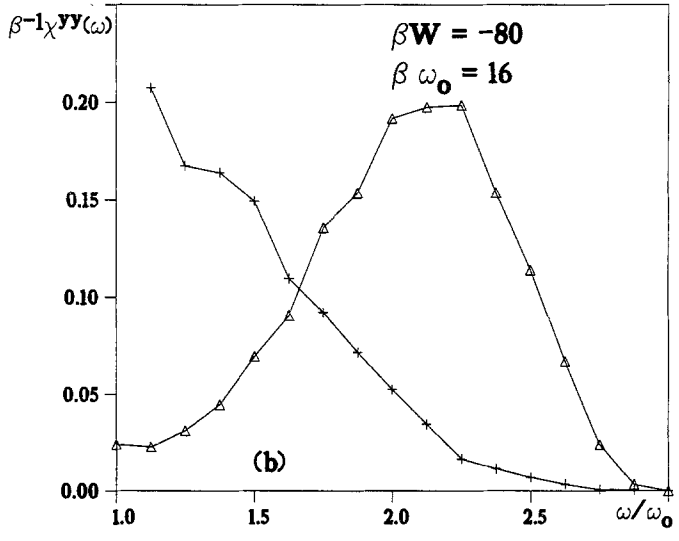

(b)

Fig. 9. Frequency-dependent susceptibility $\chi^{yy}(\omega)$ for various densities of the classical particles. (a) Nearest neighbor summation, (b) Monte Carlo simulation (symbols as in Fig. 1, connected by lines for visual guidance).

are quasiperiodic for $p \neq 0$. For times large compared to ω_0^{-1} and small compared to the spacing between the inverse frequencies, however, they show rapidly damped oscillations. For $p < 0.1$ the mean value $\bar{c}_z$ of the oscillations in C_z increases with the density, $\bar{c}_x$ decreases to values near 0, and $\bar{c}_y$ is always zero.

The reason for the apparent damping of the correlation functions is the interference between the different frequencies in Ω. For low densities the frequencies are distributed near ω_0, with some spread to higher values. When the density is increased the average frequency $\bar{\omega}$ increases, in conformity with our discussion of Eq. (2.3). This can be seen in the frequency-dependent susceptibilities such as $\chi^{yy}(\omega)$ defined in (2.12) and plotted in Fig. 9. As the Fourier transform of $\chi^{yy}(\omega)/\tanh(\beta\omega/2)$ gives the real-time correlation functions $C_y(t)$, these new frequencies give directly the apparent damped oscillatory behavior of the real-time correlation functions. Parallel results can be obtained when the interaction strength is increased instead of the density.

For larger densities ($p > 0.1$), this behavior reverses. The classical particles, in their tendency toward localizing around the position of one of the potential minima, fill all the sites there. This gives a less asymmetric potential, i.e., reduces $h(\{\mathbf{q}_j\})$, for the quantum particle, making it more like a free particle with enhanced tunneling probability. The values of $C_x(-i\beta/2)$ increase and the values of $C_z(-i\beta/2)$ decrease with increasing densities, becoming equal at a density near $p = 0.5$.

With increasing density $\bar{c}_x$ increases, $\bar{c}_z$ decreases, and the relaxation time gets larger. For densities near $p = 0.9$, the asymmetries in the potentials are nearly zero, and the oscillatory behavior of $C_x(t)$ is similar to that of the free system.

We remark here that for the lattice gas fluid the measure μ of (2.13) is invariant under $p \to 1 - p$ and $U \to -U$, so that for a repulsive interaction (2.14), $W = 5\omega_0$, the maximum hybridization occurs at p close to unity. This can be understood by noting that at low densities the repulsive interactions keep the fluid particles away from the quantum system.

We also carried out Monte Carlo calculations for the continuum fluid, taking for $\tilde{U}$ a hard-core potential. Identifying the density $\rho^* = \rho b^3$ with p gives results similar to those for the corresponding lattice system. The potential fluctuations h are, however, smaller for the hard-sphere fluid and thus the resulting localization is less pronounced.

4. PATH INTEGRAL MONTE CARLO

The real-time correlations, Figs. 6–8, and the corresponding susceptibilities, plotted in Fig. 9, are the quantities one would normally like to

extract by analytic continuation from path integral Monte Carlo. The latter can be carried out for more realistic systems to yield the imaginary time correlations $C_\alpha(-i\tau)$. We did PIMC also here by discretizing the path integral corresponding to (2.1) as in ref. 9. Then for a given configuration $\{\mathbf{q}_j\}$ of the fluid the measure on the discrete path is given by the Ising Hamiltonian

$$H_{\mathrm{cl}} = -K_L \sum_{k=1}^{L} S_k S_{k+1} + \frac{h}{2L} \sum_{k=1}^{L} S_k + \frac{1}{2} u_0 + \frac{1}{2} \sum_{\substack{i \neq j \\ i,j=1}}^{N} \tilde{U}(\mathbf{q}_i - \mathbf{q}_j) \quad (4.1)$$

where $S_k = \pm 1$, corresponding to eigenvalues of σ^z, and $K_L = (1/2\beta) \ln[\tanh(\beta\omega_0/2L)]$. We consider now H_{cl} as the energy for the "spin" degrees of freedom $\{S_k\}$ and the classical degrees of freedom $\{\mathbf{q}_j\}$ also contained in h and u_0. Annealed quantum averages are then the same as classical averages with respect to H_{cl}.

Imaginary-time correlations are obtained through the averages[9,10]

$$C_x\left(\frac{\vartheta\beta}{L}\right) = \left\langle \frac{1}{L} \sum_{k=1}^{L} \exp[-2\beta K_L (S_k S_{k+1} + S_{k+\vartheta} S_{k+\vartheta+1})] \right\rangle \quad (4.2)$$

$$C_y\left(\frac{\vartheta\beta}{L}\right) = \left\langle \frac{1}{L} \sum_{k=1}^{L} (-S_k S_{k+\vartheta}) \exp[-2\beta K_L (S_k S_{k+1} + S_{k+\vartheta} S_{k+\vartheta+1})] \right\rangle \quad (4.3)$$

$$C_z\left(\frac{\vartheta\beta}{L}\right) = \left\langle \frac{1}{L} \sum_{k=1}^{L} S_k S_{k+\vartheta} \right\rangle \quad (4.4)$$

with $\vartheta = 1, \ldots, L$.

We compare the imaginary-time correlation functions obtained by the PIMC methods with those of Section 3, especially for the density of 0.5 and $W = 5\omega_0$. We choose $L = 80$, which corresponds to about 16 correlation lengths along the β axis. An increase of L does not affect the results. A typical run with 10^7 Monte Carlo time steps took about 3 h on a VAX8600. The σ^z correlation functions along the "polymer" follow very closely the results obtained by the methods of Section 3. However, the σ^x as well as the σ^y correlations, which are related to the second derivative of the σ^z correlations, fluctuate around the exact values (obtained via diagonalization) and do not show a nice behavior (see Fig. 10).

To obtain the real-time correlations we continue the imaginary-time correlation functions to real time by the analytical continuation method of Berne *et al.*,[7] which utilizes Padé approximants. The results of this procedure depend sensitively on the quality of the imaginary-time results; small

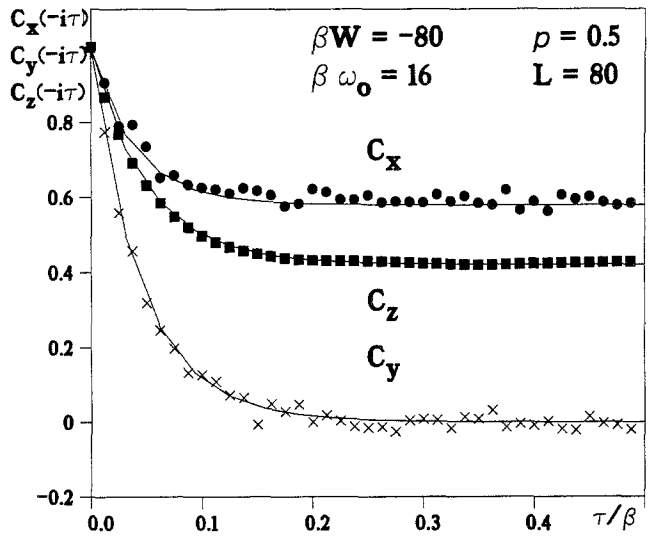

Fig. 10. Imaginary-time correlation function. Comparison of the Monte Carlo simulations utilizing the diagonalization techniques (lines) with path integral Monte Carlo (points) simulations.

deviations from the exact form in the latter can give a completely different real-time behavior. For zero interaction we obtained the oscillations of $C_z(t)$ and $C_y(t)$ with the frequency ω_0. In general the imaginary-time correlation functions are so structureless, even for the case of nonzero interaction, that we were never able to obtain more than one frequency by the Padé approximation technique. This frequency is shifted to a value near the maximum of $\chi^{yy}(\omega)$ obtained with the method of Section 2, but, as it is a single frequency, it gives only a very crude idea of what is really going on.

5. EFFECTIVE POTENTIAL

In this section we use the general imaginary-time formalism of quantum mechanics to obtain qualitative information about the localization of our system. The PIMC discussed in the last section is of course just a discretization of the Feynman–Kac formula.[11] This formula gives a measure over imaginary time paths in the interval $0 \leqslant \tau \leqslant \beta$ from which expectation values of equilibrium quantities and imaginary-time correlations can be obtained directly. For the Hamiltonian (1.2) this has the form

$$\langle A\rangle_Q = \left(\int Dq(\cdot)\, A(q) \exp\left\{-\int_0^\beta d\tau \left[\frac{1}{2} m_0 \dot{q}(\tau)^2 + V(q(\tau))\right]\right\}\right.$$
$$\times \left\langle \exp\left[-\int_0^\beta d\tau \sum_j U(q(\tau) - \mathbf{q}_j)\right]\right\rangle\Bigg)$$
$$\times \left(\int Dq(\cdot) \exp\left\{-\int_0^\beta d\tau \left[\frac{1}{2} m_0 \dot{q}(\tau)^2 + V(q(\tau))\right]\right\}\right.$$
$$\left.\times \left\langle \exp\left[-\int_0^\beta d\tau \sum_j U(q(\tau) - \mathbf{q}_j)\right]\right\rangle\right)^{-1} \tag{5.1}$$

where the sum is over all paths $q(\tau)$ with $q(0) = q(\beta)$. The first factor in the path integral is the "free part." It takes into account only the external potential V. The second factor, which is an average over the classical distribution of the fluid particles, yields an effective quantum action which, on the level of imaginary-time correlations, represents the influence of the surrounding fluid.

To obtain the two-level approximation used in Sections 2–4, we exploit the fact that our potentials V have two pronounced minima at $q_\pm = \pm 1$ related by reflection symmetry. A typical path therefore spends most of its "time" (at sufficiently low temperatures) at one or the other of the two minima. The path $q(\tau)$ may therefore be approximated by a path $\sigma(\tau)$ taking only the two values ± 1 which jumps at random times between the minima. The rate of jumping is just the tunneling frequency ω_0 given in (2.1). Thus, according to the free path measure, the path $\sigma(\tau)$ has the following statistics: the times $\{\tau_j\}$ when $\sigma(\tau)$ changes sign have a random (Poisson) distribution with density ω_0, conditioned [because $\sigma(0) = \sigma(\beta)$] so that the number of sign changes of $\sigma(\tau)$ is even. We denote this distribution of paths by $P^{\omega_0}(d\sigma(\cdot))$ (see ref. 6). In our approximation the measure in (5.1) becomes

$$\frac{1}{Z_1} P^{\omega_0}(d\sigma(\cdot)) \left\langle \exp\left[-\int_0^\beta d\tau \sum_j U(q_{\sigma(\tau)} - \mathbf{q}_j)\right]\right\rangle \tag{5.2}$$

We have to understand now how the interaction with the fluid modifies the *a priori* statistics of paths given by $P^{\omega_0}(d\sigma(\cdot))$. From (5.2) we conclude that the classical average $\langle\cdot\rangle$ depends on $\sigma(\tau)$ only through the "magnetization" per unit length,

$$m = \frac{1}{\beta}\int_0^\beta d\tau\, \sigma(\tau) \tag{5.3}$$

Therefore, let us define the classical part of the action by

$$\begin{aligned} S_c(m) &= -\ln \left\langle \exp\left[-\int_0^\beta d\tau \sum_j U(q_{\sigma(\tau)} - \mathbf{q}_j) \right] \right\rangle \\ &= -\ln \left\langle \exp\left\{ -\frac{1}{2}\int_0^\beta d\tau \, [u_0 - h\sigma(\tau)] \right\} \right\rangle \\ &= -\ln \left\langle \exp\left[-\frac{\beta}{2}(u_0 - mh) \right] \right\rangle \end{aligned} \tag{5.4}$$

with h and u_0 as in (2.2). S_c can be thought of as a mean field interaction for the Ising model. Unlike the standard example of a mean field interaction $-Jm^2$, $S_c(m)$ is in general not quadratic. It is, however, concave (bent downward), with the second derivative at $m=0$ given by $-\langle(\beta h/2)^2\rangle$. It is also symmetric around $m=0$ as a consequence of the symmetry of the distribution of h, since $U(\mathbf{q})$ is even.

The distribution of the magnetization m according to (5.2) is given by

$$\frac{1}{Z_I} e^{-S_q(m) - S_c(m)} \tag{5.5}$$

where

$$e^{-S_q(m)} = \int P^{\omega_0}(d\sigma(\cdot)) \, \delta\left(m - \frac{1}{\beta}\int_0^\beta d\tau \, \sigma(\tau) \right) \tag{5.6}$$

$S_q(m)$ is essentially the Helmholtz free energy of the (continuum) Ising system as a function of the magnetization. Taking the Laplace transform of (5.6) yields

$$\int_{-1}^{1} dm \, e^{-S_q(m)} e^{-\lambda m} = 2\cosh\left[\left(\frac{\beta\omega_0}{2} \right)^2 + \lambda^2 \right]^{1/2} \tag{5.7}$$

(5.7) cannot be inverted explicitly. For large β we can use the method of steepest descent and obtain

$$S_q(m) \sim -\tfrac{1}{2}\beta\omega_0(1-m^2)^{1/2} \tag{5.8}$$

Thus, we may understand the statistics of the paths as a competition between random flipping ($\triangleq S_q$) which wants to keep $m=0$ and the classical action S_c, which prefers $m=\pm 1$.

There are two cases where the classical action can be calculated without effort. The virtue of these examples is to demonstrate again that localization is due to large potential fluctuations.

(i) There is no interaction between the fluid particles, $\tilde{U}=0$. The classical particles are then distributed as an ideal gas with density ρ. This yields a simple exponential for the average in (5.4),[12] giving

$$S_c(m)=\rho\int d\mathbf{q}\left[1-\exp\left\{m\frac{\beta}{2}[U(q_- -\mathbf{q})-U(q_+ -\mathbf{q})]\right.\right.$$
$$\left.\left.-\frac{\beta}{2}[U(q_+ -\mathbf{q})+U(q_- -\mathbf{q})]\right\}\right] \tag{5.9}$$

Using the general properties of S_c, it suffices to look at

$$S_c(0)-\frac{1}{2}S_c(1)-\frac{1}{2}S_c(-1)$$
$$=\frac{\rho}{2}\int d\mathbf{q}\left\{\exp\left[-\frac{\beta}{2}U(q_+ -\mathbf{q})\right]-\exp\left[-\frac{\beta}{2}U(q_- -\mathbf{q})\right]\right\}^2 \tag{5.10}$$

Therefore, if $U\geqslant 0$, $S_c\to 0$ exponentially as $\beta\to\infty$. On the other hand, if the minimum of U is negative, then the difference (5.10) increases exponentially and the quantum particle localizes at $q_\pm$ as $\beta\to\infty$.

The physical mechanism is best understood through the distribution of classical particles. If $U\geqslant 0$, then typically the classical particles are pushed away from the quantum particle and in the limit $\beta\to\infty$ no effect of the interaction with the fluid remains. If, on the other hand, U has an attractive part, then since we have assumed that there is no hard core, particles pile up at the minimum of $U(\mathbf{q}-q_\pm)$. This is associated with large fluctuations which make the potential seen by the quantum particle typically very asymmetric—hence it effectively localizes.[4–6]

(ii) As in our numerical simulation, we assume that the classical particles are located at the sites of a simple cubic lattice with lattice constant b with at most one particle per site. We assume that there is no other interaction between the classical particles, so that a site is independently occupied with probability p, $0\leqslant p\leqslant 1$. For this hard-core lattice gas the classical part of the action becomes

$$S_c(m)=-\sum_{j\in(b\mathbb{Z})^3}\{\ln[(1-p)e^{F(j)}+pe^{-F(j)}]-F(j)\} \tag{5.11}$$

where

$$F(j)=\frac{\beta}{4}[U(q_- -j)+U(q_+ -j)-m[U(q_- -j)-U(q_+ -j)]] \tag{5.12}$$

Let us again consider the limit of large β. If $U\leqslant 0$ (or, by symmetry, if $U\geqslant 0$), then the situation is just as before; for fixed p, particles are either

pulled in and occupy all available lattice sites close to the quantum particle or are pushed away and one is back to free tunneling; compare with the effect of fluctuations displayed in Fig. 5. To maintain potential fluctuations, we have to let $p \to 0$ simultaneously with $\beta \to \infty$. Another way to ensure potential fluctuations is to make U repulsive at short distances and attractive at large distances. To see this, we take the large-β limit in (5.11). $S_c(m)$ converges then to

$$\beta S(m) = 2 \sum_j F(j)\, \theta(F_j) \tag{5.13}$$

plus a constant independent of m with $\theta(F) = 1$ if $F \leqslant 0$ and $\theta(F) = 0$ if $F > 0$. If either $U \geqslant 0$ or $U \leqslant 0$, then $S(m) = \text{const}$. However, if U has both signs, because of "screening" one can achieve that $S(0) > S(1)$. By (5.8) for large β the full action is given by

$$S_q(m) + S_c(m) \cong \beta[-\omega_0(1-m^2)^{1/2} + S(m)] \tag{5.14}$$

which for an appropriate choice of the parameters in the potential has its minimum at $\pm\bar{m} \neq 0$. Hence, the quantum particle localizes fully in one of the minima as $\beta \to \infty$.

6. CONCLUDING REMARKS

We studied the behavior of a two-level quantum particle in equilibrium with a classical heat bath. This model for a quantum particle in a double-well potential interacting with classical particles allows the study of correlation functions in real and imaginary time as well as the frequency-dependent susceptibility when the density of the classical system is varied. The main advantage of the two-level approximation is that the quantum mechanical expectation values can be obtained exactly for arbitrary classical configurations. The remaining average over the classical distribution can then be performed by the methods of classical statistical mechanics—by exact analytic calculation in a few simple cases, otherwise by Monte Carlo methods.

Using analytic methods for a simple model where the classical particles were confined to a lattice, we obtained increasing damping and frequency shifts in the time correlation functions of the quantum system with increasing densities up to a density near 0.1. At higher densities the classical particles occupy all the places around the possible quantum positions; the resulting potential is then essentially independent of the state of the quantum particle and thus the tendency to localize gets smaller, and so do the damping and frequency shifts.

In addition to this semianalytical evaluation of relevant observables, we compared the imaginary-time correlation functions with the corresponding correlations obtained by path integral Monte Carlo simulations. The purpose of this was to see if the PIMC imaginary-time correlation functions can be found accurate enough to allow for the continuation of these functions to real time. The answer turned out to be that we could get only restricted real-time information from PIMC. The very small noise in the PIMC imaginary-time results caused such a loss of information about the dynamical behavior of the quantum particle that only one frequency could be found with the usual Padé approximation technique. This frequency, however, is in fact near the maximum for the susceptibility and so gives the correct average behavior of the system.

The results show the convenience of the two-level approximation for the study of time-dependent phenomena in a quantum system interacting with a classical environment. A more sophisticated treatment of this problem involving the solution of the Schrödinger equation for the Hamiltonian (1.2) to obtain the two lowest eigenfunctions is in progress.

ACKNOWLEDGMENTS

We gratefully acknowledge useful discussions and correspondence with Oliver Penrose and Shalom Baer, and the computational support of the John von Neumann Supercomputer Center.

P. N. was supported by Postdoktoranden Stipendium der Deutschen Forschungsgemeinschaft. The research of J. L. L., H. S., and J. L. V. was supported in part by AFOSR grant No. 86-0010 and by Applied Mathematical Sciences subprogram of the Office of Energy Research, U.S. DOE under contract No. DE-FG02-88ER25053. J. L. V. was also supported in part by U.S./Spain Joint Committee Research grant No. CCB-8402-025 and by the CIRIT de la Generalitat de Catalunya, Spain.

REFERENCES

1. D. Chandler and P. G. Wolynes, *J. Chem. Phys.* **74**:4078 (1981); J. S. Hoye and G. Stell, *J. Chem. Phys.* **75**:5133 (1981); D. Chandler, *Introduction to Modern Statistical Mechanics* (Oxford University Press, New York, 1987).
2. M. Sprik, R. W. Impey, and M. L. Klein, *Phys. Rev. Lett.* **56**:2326 (1986); D. F. Coker, B. J. Berne, and D. Thirumalai, *J. Chem. Phys.* **86**:5689 (1987); Y. Chung, P. Lemaire, and S. Suckewer, *Phys. Rev. Lett.* **60**:1122 (1988).
3. I. Messing, B. Raz, and J. Jortner, *J. Chem. Phys.* **66**:2239, 4577 (1977); R. Nowak and E. R. Bernstein, *J. Chem. Phys.* **87**:2457 (1987); N. Schwentner, E.-E. Koch, and J. Jortner, *Electronic Excitations in Condensed Rare Gases* (Springer-Verlag, Berlin, 1985).

4. P. Claverie and G. Jona-Lassinio, *Phys. Rev. A* **33**:2245 (1986); B. Bleaney, J. H. N. Loubser, *Nature* **161**:522 (1948).
5. A. J. Leggett, S. Chakravarty, A. T. Dorsay, M. P. A. Fisher, A. Garg, and W. Zwerger, *Rev. Mod. Phys.* **59**:1 (1987).
6. H. Spohn and R. Dümke, *J. Stat. Phys.* **41**:389 (1985).
7. D. Thirumalai and B. Berne, *J. Chem. Phys.* **79**:5029 (1983); J. D. Doll, R. D. Coalson, and D. L. Freeman, *J. Chem. Phys.* **87**:1641 (1987); J. Chang and W. H. Miller, *J. Chem. Phys.* **87**:1648 (1987); J. D. Doll, T. L. Beck, and D. L. Freeman, preprint.
8. R. Kubo, *J. Phys. Soc. Japan* **12**:149 (1957); R. Kubo, M. Toda, and N. Hashitsume, *Statistical Physics II* (Springer-Verlag, Berlin, 1985).
9. P. Ballone, P. de Smedt, J. L. Lebowitz, J. Talbot, and E. Waisman, *Phys. Rev. A* **35**:2 (1987); P. de Smedt, P. Nielaba, J. L. Lebowitz, J. Talbot, and L. Dooms, *Phys. Rev. A* **38**:1381 (1988).
10. M. Suzuki, *Prog. Theor. Phys.* **46**:1337 (1971), **56**:1454 (1976); *Commun. Math. Phys.* **51**:183 (1976).
11. R. P. Feynman and A. R. Hibbs, *Quantum Mechanics and Path Integrals* (McGraw-Hill, New York, 1965).
12. T. Burke and J. L. Lebowitz, *J. Math. Phys.* **9**:1586 (1968).